

# High-Accuracy Calculations of the Critical Exponents of Dyson's Hierarchical Model

J. J. Godina

*Dep. de Fis. , CINVESTAV-IPN , Ap. Post. 14-740, Mexico, D.F. 07000  
and Dpt. of Physics and Astr., Univ. of Iowa, Iowa City, Iowa 52242, USA*

Y. Meurice and M. B. Oktay

*Dpt. of Physics and Astr., Univ. of Iowa, Iowa City, Iowa 52242, USA*

We calculate the critical exponent  $\gamma$  of Dyson's hierarchical model by direct fits of the zero momentum two-point function calculated with an Ising and a Landau-Ginzburg measure, and by linearization about the Koch-Wittwer fixed point. We find  $\gamma = 1.299140730159 \pm 10^{-12}$ . We extract three types of subleading corrections (in other words, a parametrization of the way the two-point function depends on the cutoff) from the fits and check the value of the first subleading exponent from the linearized procedure. We suggest that all the non-universal quantities entering the subleading corrections can be calculated systematically from the non-linear contributions about the fixed point and that this procedure would provide an alternative way to introduce the bare parameters in a field theory model.

## I. INTRODUCTION

Scalar field theory has many important applications in condensed matter and particle physics. Unfortunately, there exists no approximate treatment of this theory which could pretend to compete in accuracy with perturbative methods in quantum electrodynamics at low energy. Accurate calculations of subtle effects at accessible energies provide a window on hypothetical high energy degrees of freedom which are not accessible by production experiments. If we imagine for a moment that the kaons were the heaviest particles that we could produce, a precise determination of their weak matrix elements would become a unique way to obtain a quantitative information about the charmed quark. Rescaled versions of this imaginary situation may become relevant in the future.

The main goal of this article is to demonstrate that the use of hierarchical approximations allows determinations of the renormalized quantities, with an accuracy which can compete with perturbative QED, and for a wide range of UV cutoff and bare parameters. The use of hierarchical approximations simplifies the renormalization group (RG) transformation while preserving the qualitative features of scalar field theory. Well-known examples are the approximate recursion formula derived by K. Wilson [1], or the related recursion formula which holds for Dyson's hierarchical model [2]. If used for quantitative purposes, hierarchical approximations need to be improved. This is a difficult task under investigation and which is not discussed here. If the hierarchical approximation could be improved in a way which maintain the advantages of the approximation, one could obtain results with an accuracy which would outperform any Monte Carlo method and defy any experimental patience.

In the following, we use the scaling laws [3] to express

the renormalized quantities as function of the bare quantities and a UV cut-off. This parametrization (see e.g., Eqs. (1.4) and (1.6)) is motivated below. We show with an example that the unknown parameters entering in the scaling laws can be determined accurately. In particular, one universal quantity entering in the scaling law associated with the two point function (the critical exponent  $\gamma$ ) can be calculated with two independent methods with an agreement in the 12-th decimal point. These two methods were sketched in Ref. [4]. In the meantime, these methods were improved in order to get a significantly better accuracy. A detailed description of these two methods is the main technical content of the present paper.

All the calculations reported in this paper were made with a specific example selected for its simplicity. However, there is nothing essential in the choice of this example and accurate calculations can be performed with the same tools in a much broader range of models and parameters. For the sake of definiteness we now describe the example chosen hereafter. We have limited the discussion to a calculation of the zero-momentum two point function of Dyson's hierarchical model with a one-component scalar field and with a choice of the free parameter (denoted  $c$ ) which approximates a  $D = 3$  theory. We considered a wide range of UV cutoff (14 orders of magnitude) and two different sets of bare parameters. The choice of the hierarchical model is not essential either. Wilson's approximate recursion formula is closely related to the recursion formula appearing in Dyson's hierarchical model [2]. It is possible to continuously interpolate between the critical exponents of the two cases [5]. The numerical treatment of the two cases is completely identical. We have specialized the discussion to the case of Dyson's model because this model has been studied [6–10] in great detail in the past and because a fixed point of this model at  $D = 3$  is known with great precision [7]. For the sake

of completeness the main features of Dyson's model are reviewed in section II A. The choice of the two-point function is not essential. The methods can be extended to other renormalized quantities as explained in Ref. [10].

The goal of a typical field theory calculation, is to obtain the renormalized quantities corresponding to the bare parameters entering in an action and a given UV cut-off  $\Lambda$ . In the following calculations, the bare parameters will appear in a local measure of the Landau-Ginzburg (LG) form:

$$W_0(\phi) \propto \exp\left(-\left(\frac{1}{2}m^2\phi^2 + g\phi^{2p}\right)\right). \quad (1.1)$$

The UV cut-off corresponds to the scale where the theory under consideration stops being an accurate description and a more complete or more fundamental theory is required. Given a set of bare parameters and a UV cutoff  $\Lambda$ , one can try to integrate [1] the degrees of freedom between  $\Lambda$  and a lower energy scale of reference  $\Lambda_R$  in order to obtain an effective theory describing phenomena at scales below  $\Lambda_R$ . As an example, if we are interested in low energy processes involving pions,  $\Lambda$  could be chosen around  $m_\rho$  and  $\Lambda_R$  around  $m_\pi$ . This gives a ratio of about 6 between the two scales. Similar ratios may be applicable for an effective description of the Higgs boson in the hypothetical case that it results from an underlying strongly interacting theory. If we are interested in the effects of the charmed quarks in non-leptonic decays of kaons, the ratio of the two scales would approximately be 3. Larger ratios appear if, for instance, we are interested in the effects of the top quark in systems involving only the five other quarks, or the effects of the  $W$  and  $Z$  gauge bosons on the propagation of an electron in a constant magnetic field. From these examples it is clear that one would like to be able to cover a wide range of values of  $\Lambda_R/\Lambda$ .

In the scalar theory under consideration here, the cut-off is lowered by discrete steps which reduce the initial cutoff by a factor  $2^{-\frac{1}{D}}$  for a “ $D$ -dimensional” theory (the notion of dimensionality is explained at length in section II C). The limit of a large UV cut-off  $\Lambda$  can be reached by fine-tuning  $\beta$ , the inverse temperature in Dyson's formulation of the model [2]. We use here the statistical mechanics language: the magnetic susceptibility  $\chi$  is studied by varying  $\beta$ , keeping the bare parameters fixed. We could have, in a completely equivalent way, called the susceptibility the zero momentum two point function, set  $\beta$  – the kinetic term coupling constant – equal to one and fine-tuned the bare mass.

We now follow Ref. [1] and consider a sequence  $L = 1, 2, \dots$  of models with  $\beta = (\beta_c - \lambda_1^{-L}\mu)$  where  $\lambda_1$  is the largest eigenvalue of the linearized renormalization group transformation and  $\mu$  an arbitrary positive parameter. If we consider a fixed value of  $L$  and if  $\mu$  is of order one, it takes about  $L$  iterations of the renormalization group transformation to get an effective theory with a mass of order one in  $\Lambda_R$  units. This comes from the fact that in the linearized approximation (see IID),  $\beta_c - \beta$  measures

how far we are away from the stable manifold [3] and this quantity is multiplied by  $\lambda_1$  at each iteration until it reaches a value of order one and the linearization does not hold any more. This suggests the definition of the renormalized mass  $m_R^2$ :

$$m_R^2 = \frac{\Lambda_L^2}{\chi(\beta_c - \lambda_1^{-L}\mu)}, \quad (1.2)$$

where  $\Lambda_L$  is the UV cut-off defined as

$$\Lambda_L = 2^{\frac{L}{D}} \Lambda_R. \quad (1.3)$$

For  $\beta$  close enough to  $\beta_c$  (i.e., for  $\Lambda$  large enough), one can approximate the susceptibility with an expression which, when  $D < 4$ , takes the form [3]

$$\chi \simeq (\beta_c - \beta)^{-\gamma} (A_0 + A_1(\beta_c - \beta)^\Delta + \dots), \quad (1.4)$$

where  $A_0, A_1, \dots$  are functions of the bare parameters only. From the above equations and the expression of  $\gamma$  given in Eq. (2.17) which implies

$$\lambda^\gamma = 2^{\frac{2}{D}}, \quad (1.5)$$

one obtains

$$m_R^2 = \frac{\Lambda_R^2 \mu^\gamma}{A_0 + A_1 \left(\frac{\Lambda_R}{\Lambda_L}\right)^{\frac{\Delta}{2\gamma}} + \dots}. \quad (1.6)$$

The main technical endeavor pursued in this article is to determine numerically the unknown quantities in Eq. (1.4) and to determine the nature of the next corrections. We have used two independent methods. The first one consists in fitting the susceptibility at various values of  $\beta$  using Eq. (1.4). The second method consists in calculating the eigenvalues of the linearized renormalization group transformation in order to determine the critical exponents. The present article contains the details of the results announced in Ref. [4]. In the meantime we have refined some of the procedures used previously and improved significantly the accuracy of our results (e.g., at least four more significant digits in  $\gamma$ ). These refinements are reported in the present article.

The first estimation of the unknown quantities is based on a method of calculation presented in Ref. [10] where it is shown that the use of polynomial approximations in the Fourier transform of the recursion relation allows efficient and highly accurate calculations of the zero-momentum Green's functions in the symmetric phase. The method is reviewed in section II where we also justify the introduction of a dimensionality parameter and review the linearization procedure. In section III, we analyze the errors associated with the method. We first explain how to get rid of the volume effects for the range of temperature considered later. We then analyze the round-off errors in arithmetic operations and show how to reduce them to an acceptable level by the use higher precision arithmetic, when necessary. We then discuss the effects of the

polynomial truncations and of the numerical errors in the calculation of the Fourier transform of the measure given by Eq. (1.1) and show that they can be reduced to a level where they will play no role in the discussion which follows. We conclude the section with an explanation of why a great numerical accuracy can only be achieved in the symmetric phase.

In section IV, we fit the susceptibility with the four parameters appearing in Eq. (1.4), neglecting the next subleading corrections indicated by the  $+\dots$ . After four successive refinements, all based on reproducible linear fits, we obtain values of  $\gamma$  with a numerical stability up to the 13-th decimal point. In section V we analyze the next subleading corrections and show that neglecting them affects slightly the 12-th decimal point in  $\gamma$ . All the calculations in these two sections have been done with two different measures and gave compatible results for the universal quantities ( $\gamma$  and  $\Delta$ ).

The most efficient way to calculate the critical exponent  $\gamma$  and  $\Delta$  consists in using the linearized renormalization group transformation [3] near a fixed point. This is done explicitly in section VI. In ref. [4], we gave convincing arguments indicating the uniqueness of the non-trivial fixed point for a large class of theories. In this article, we take this uniqueness for granted and we use the very accurate expression of this fixed point obtained from the work of Koch and Wittwer [7] rather than the less accurate fixed points used in Ref. [4]. This allows us to obtain values of  $\gamma$  with estimated errors of less than one in the 13-th significant digit, the actual value agreeing with the previous estimate within the expected uncertainties.

If there is only one non-trivial fixed point (universality) and if we can calculate accurately the exponents, the task of calculating the renormalized quantities for a particular set of bare parameters reduces to the determination of quantities like  $A_0, A_1, \dots$ . This task can be achieved by repeated subtractions as shown in sections IV and V. We are convinced that such calculations could be performed more efficiently by using the fixed point and a calculation of the nonlinear effects. We have checked [11] that such a calculation can be satisfactorily performed in simplified versions of the basic recursion relation. If this task can be successfully completed for the model considered here, this would mean that the precise knowledge of the fixed point provided by Ref. [7] is equivalent to a solution of the model.

An accurate determination of the universal exponents provides a new approach of the renormalization procedure: we could try to treat as much as possible of the  $A_0, A_1, \dots$  and the corresponding quantities for the higher point functions as *input* parameters. This of course suppose that we have a detailed knowledge of their relative dependences. This question is under investigation with various methods.

## II. THE MODEL AND THE CALCULATION OF THE SUSCEPTIBILITY

In this section, we describe the method used to calculate the magnetic susceptibility and introduce some definitions which will be used later. For the sake of being self-contained, we first recall basic facts about Dyson's Hierarchical Model [2].

### A. Dyson's Model

The model has  $2^{n_{max}}$  sites. We label the sites with  $n_{max}$  indices  $x_{n_{max}}, \dots, x_1$ , each index being 0 or 1. In order to understand this notation, one can divide the  $2^{n_{max}}$  sites into two blocks, each containing  $2^{n_{max}-1}$  sites. If  $x_{n_{max}} = 0$ , the site is in the first box, if  $x_{n_{max}} = 1$ , the site is in the second box. Repeating this procedure  $n$  times (for the two boxes, their respective two sub-boxes, etc.), we obtain an unambiguous labeling for each of the sites.

The non local part of the action of Dyson's Hierarchical model reads

$$H = -\frac{\beta}{2} \sum_{n=1}^{n_{max}} \left(\frac{c}{4}\right)^n \sum_{x_{n_{max}}, \dots, x_{n+1}} \left( \sum_{x_n, \dots, x_1} \phi_{(x_{n_{max}}, \dots, x_1)} \right)^2. \quad (2.1)$$

The index  $n$ , referred to as the 'level of interaction' hereafter, corresponds to the interaction of the total field in blocks of size  $2^n$ . The constant  $c$  is a free parameter which control the decay of the iterations with the size of the boxes and can be adjusted in order to mimic a  $D$ -dimensional model. This point is discussed in more detail below.

The field  $\phi_{(x_{n_{max}}, \dots, x_1)}$  is integrated over a local measure which needs to be specified. In the following, we will work with the Ising measure,  $W_0(\phi) = \delta(\phi^2 - 1)$  and the Landau-Ginsburg measure of the form given in Eq. (1.1). The hierarchical structure of Eq. (2.1), allows us to integrate the fields while keeping their sums in boxes with 2 sites. This can be expressed through the recursion relation

$$W_{n+1}(\phi) = \frac{C_{n+1}}{2} e^{(\beta/2)(c/4)^{n+1} \phi^2} \times \int d\phi' W_n\left(\frac{\phi - \phi'}{2}\right) W_n\left(\frac{\phi + \phi'}{2}\right), \quad (2.2)$$

where  $C_{n+1}$  is a normalization factor which can be fixed at our convenience.

### B. Polynomial Truncations

Introducing the Fourier representation

$$W_n(\phi) = \int \frac{dk}{2\pi} e^{ik\phi} \widehat{W}_n(k), \quad (2.3)$$

and a rescaling of the source by a factor  $1/s$  at each iteration, through the redefinition

$$R_n(k) = \widehat{W}_n\left(\frac{k}{s^n}\right), \quad (2.4)$$

the recursion relation becomes

$$R_{n+1}(k) = C_{n+1} \exp\left(-\frac{1}{2}\beta\left(\frac{c}{4}s^2\right)^{n+1} \frac{\partial^2}{\partial k^2}\right) \left(R_n\left(\frac{k}{s}\right)\right)^2. \quad (2.5)$$

The rescaling operation commutes with iterative integrations and the rescaling factor  $s$  can be fixed at our convenience.

We will fix the normalization constant  $C_n$  in such way that  $R_n(0) = 1$ . Then,  $R_n(k)$  has a direct probabilistic interpretation. If we call  $M_n$  the total field  $\sum \phi_x$  inside blocks of side  $2^n$  and  $\langle \dots \rangle_n$  the average calculated without taking into account the interactions of level strictly larger than  $n$ , we can write

$$R_n(k) = \sum_{q=0}^{\infty} \frac{(-ik)^{2q} \langle (M_n)^{2q} \rangle_n}{2q! s^{2qn}}. \quad (2.6)$$

We see that the Fourier transform of the local measure after  $n$  iterations generates the zero-momentum Green's functions calculated with  $2^n$  sites and can thus be used to calculate the renormalized mass and coupling constant at zero momentum.

In the following, we use finite dimensional approximations of degree  $l_{max}$  of the form:

$$R_n(k) = 1 + a_{n,1}k^2 + a_{n,2}k^4 + \dots + a_{n,l_{max}}k^{2l_{max}}. \quad (2.7)$$

After each iteration, non-zero coefficients of higher order ( $a_{n+1,l_{max}+1}$  etc.) are obtained, but not taken into account in the next iteration. More explicitly, the recursion formula for the  $a_{n,m}$  reads :

$$a_{n+1,m} = \frac{\sum_{l=m}^{l_{max}} (\sum_{p+q=l} a_{n,p} a_{n,q}) [(2l)! / (l-m)! (2m)!] (c/4)^l [-(1/2)\beta]^{l-m}}{\sum_{l=0}^{l_{max}} (\sum_{p+q=l} a_{n,p} a_{n,q}) [(2l)! / l!] (c/4)^l [-(1/2)\beta]^l}. \quad (2.8)$$

As one can see that once an initial  $R_0(k)$  is given, the procedure is purely *algebraic*. The initial conditions for the Ising measure is  $R_0(k) = \cos(k)$ . For the LG measure, the coefficients in the  $k$ -expansion need to be evaluated numerically. This method has been discussed and tested at length in Ref. [10]. The dimension  $l_{max}$  of the polynomial spaces required to make reasonably accurate calculation is remarkably small: less than 50 for a typical calculation (see Ref. [10] for details).

As far as numerical calculations are concerned, the choice of  $s$  is a matter of convenience. For the calculations in the high temperature phase (symmetric phase) not too close to the critical points, or for high temperature expansions the choice  $s = \sqrt{2}$  works well [8,9]. On the other hand, the choice of rescaling factor  $s = 2c^{-1/2}$  prevents the appearance of very large numbers when we are very close to the critical temperature. In the following, the finite volume magnetic susceptibility is defined as

$$\chi_n(\beta) = \frac{\langle (M_n)^2 \rangle_n}{2^n}. \quad (2.9)$$

From Eq. (2.6), we obtain

$$\chi_n = -2a_{n,1} \left(\frac{s^2}{2}\right)^n. \quad (2.10)$$

### C. Introducing the Dimensionality

From a conceptual point of view, the choice  $s = 2c^{-1/2}$  is of particular significance because the infinite volume

action given in Eq.(2.1) is invariant under the removal of the  $l = 1$  terms (first level interactions) followed by the rescaling of the fields. In other words, the kinetic term is not renormalized and  $\eta = 0$ . From this, we can derive the way  $c$  should be tuned in order to mimic a  $D$ -dimensional system. Given that the dimension of a scalar field in  $D$ -dimension is  $[\phi] = [L]^{-\frac{(D-2)}{2}}$  where  $L$  is a length, we obtain in the continuum

$$\left[\left(\int d^D x \phi(x)\right)^2\right] = L^{D+2}. \quad (2.11)$$

On the lattice this becomes

$$\left[\langle (M_n)^2 \rangle_n\right] = L^{D+2}. \quad (2.12)$$

If we use the rescaling factor  $s = 2c^{-1/2}$ , the non-local part of the action given in Eq. (2.1) is invariant under a renormalization group transformation. If in addition the local measure is also left invariant, the average values of the even powers of the *rescaled* field stays constant. Returning to the original field variables, we found that at (or sufficiently close to) a fixed point,

$$\langle (M_n)^2 \rangle_n \propto \left(\frac{4}{c}\right)^n. \quad (2.13)$$

The only relevant scale is the size of the box over which we have integrated all the field variables except for their sum. The volume of the box is proportional to the number of sites inside the box:

$$L^D \propto 2^n. \quad (2.14)$$

Using this together with Eqs. (2.12) and (2.13) we obtain

$$\frac{4}{c} = 2^{\frac{1}{D} + 2}, \quad (2.15)$$

or in other words,  $c = 2^{1 - \frac{2}{D}}$ .

All the calculations done hereafter have been done for  $D = 3$ .

#### D. Review of the Linearization Procedure

We now briefly review the linearization procedure. We denote the eigenvalues of the linearized RG transformation by  $\lambda_n$  with the convention  $\lambda_1 > 1 > \lambda_2 > \lambda_3 \dots$ . The closeness to the fixed point is essentially monitored by the motion along the unstable direction. Until the number of iterations  $n$  reaches a value  $n^*$  such that  $\lambda_1^{n^*}(\beta_c - \beta) \sim 1$ ,  $R_n$  is “close” to the fixed point and  $a_{n,1}$  stays close to its fixed point value (assuming that we use the scaling factor  $s = \frac{2}{\sqrt{c}}$ ). When  $n$  gets larger than  $n^*$ ,  $\chi$  starts stabilizing. Using the relation between  $a_{n,1}$  and  $\chi_n$  given by Eq. (2.10), we obtain the order of magnitude estimate:

$$\chi \sim \left(\frac{2}{c}\right)^{n^*} = (\beta_c - \beta)^{-\frac{\ln(\frac{2}{c})}{\ln(\lambda_1)}}. \quad (2.16)$$

Reexpressing in terms of  $(\beta_c - \beta)$ , we find that the exponent for the leading singularity is

$$\gamma = \ln\left(\frac{2}{c}\right) / \ln(\lambda_1). \quad (2.17)$$

According to the same linear argument, the order of magnitude of the components in the stable directions should be proportional to  $\lambda_l^{n^*}$  with  $l \geq 2$ . Using the estimate for  $n^*$  and reexpressing in terms of  $(\beta_c - \beta)$ , we obtain the subleading exponents  $\Delta_l = -\ln(\lambda_l) / \ln(\lambda_1)$  for  $l \geq 2$ . In the following we simply use the notation  $\Delta$  for  $\Delta_2$  and the higher exponents will play no significant roles.

### III. ERROR ANALYSIS

There are three important sources of errors which need to be considered when we calculate the magnetic susceptibility: the finite volume effects, the round off errors and the effects of the finite dimensional truncation. A general discussion of these questions is given in Ref. [10]. In the following, we discuss them in the particular cases required for the calculations of section IV. In addition, we discuss the effects of the errors on the initial coefficients. All the calculations done hereafter have been made in the symmetric phase. In the last subsection, we explain why the present methods do not yield accurate results in the broken symmetry phase.

#### A. Volume Effects

As explained in IID, when calculating the susceptibility at values of  $\beta$  close to and below  $\beta_c$ , we spend about  $-\ln(\beta_c - \beta) / \ln(\lambda_1)$  iterations near the fixed point. During these iterations, we have the “conformal” scaling of Eq.(2.13) and the round-off errors are amplified along the unstable direction (see next subsection). After that, assuming we are in the symmetric phase, the order of magnitude of the susceptibility stabilizes and the corrections get smaller by a factor  $\frac{c}{2}$  at each iterations. At some point, all the recorded digits stabilize (irrespective of the numerical errors which occurred in the first stage described above). This give the estimate [10] for the number of iterations  $n(\beta, P)$  to stabilize  $P$  digits (in decimal notations)

$$n(\beta, P) = \left(\frac{D \ln(10)}{2 \ln(2)}\right) [P - \gamma \log_{10}(\beta_c - \beta)]. \quad (3.1)$$

For  $P = 16$ ,  $\gamma \simeq 1.3$  and  $\beta_c - \beta = 10^{-9}$ , we obtain  $n \simeq 140$  and we need to add about 7 iterations each time we get closer to  $\beta_c$  by a factor  $10^{-1}$ . It is thus quite easy to get rid of the volume effects. In the following, we will perform calculation  $\beta < \beta_c - 10^{-14}$  and  $n_{max} = 180$  will be enough to avoid finite volume effects.

#### B. Numerical Errors

From Eq.(2.8), we see that the calculation of each of the  $a_{n+1,l}$  involves a number of arithmetical operations proportional to  $l_{max}$ . When we are close to the fixed point, these errors generate small contributions in the unstable direction. These errors are then amplified by a factor  $\lambda_1$  at each iteration until we move sufficiently far away from the fixed point. Consequently, the closer  $\beta$  is to  $\beta_c$ , the more time is spent near the fixed point and the larger the numerical error become. A simple calculation [10] corresponding to this reasoning shows that the relative errors obey the approximate law

$$\left|\frac{\delta\chi}{\chi}\right| \sim \frac{\delta}{\beta_c - \beta}, \quad (3.2)$$

where  $\delta$  is a typical round-off error.

A simple way to probe the numerical errors is to make a small change in the rescaling factor  $s$ . As explained in the previous section, we can in principle use any value of  $s$  to calculate the susceptibility. This arbitrariness is compensated at the end by an appropriate rescaling given in Eq. (2.10). If we could perform the arithmetic operations exactly, the susceptibility would be completely independent of  $s$ . However, due to the round-off errors, the susceptibility actually depends on  $s$ . This is illustrated in Fig. 1 where we calculated the distribution of  $\chi$  for values of  $s$  varying between  $\frac{2}{\sqrt{c}} - 0.0001$  and  $\frac{2}{\sqrt{c}} + 0.0001$  by step of  $10^{-7}$

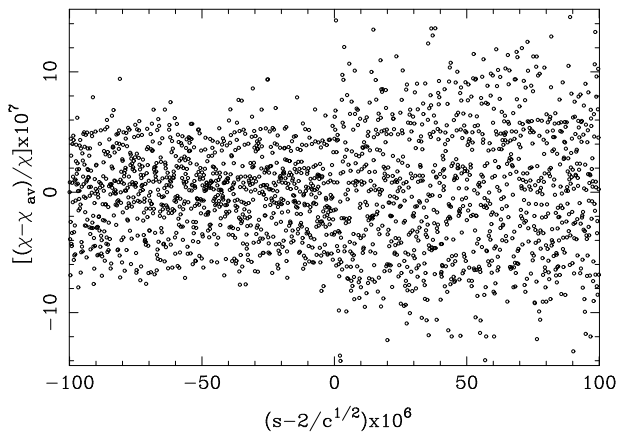


FIG. 1. Distribution of the magnetic susceptibility  $\chi$  with respect to the scaling factor  $s$ .

This calculation has been performed in Fortran with double precision variables. We have used an initial Ising measure with  $\beta = \beta_c - 10^{-9}$ . This distribution has a mean value  $\mu = 1.041926904 \times 10^{12}$  and a variance  $\sigma = 4.9 \times 10^5$ . From these quantities, we estimate that the relative errors  $|\frac{\delta\chi}{\chi}|$  due to numerical errors should be of order  $\sigma/\mu = 4.7 \times 10^{-7}$ . This is in agreement with the order of magnitude estimate of Eq. (3.2): using  $10^{-16}$  as a typical round-off error in a double-precision calculation, we obtain  $|\frac{\delta\chi}{\chi}| \sim 10^{-7}$  for  $\beta_c - \beta = 10^{-9}$ . A more accurate calculation performed with methods described below gives the result  $\chi = 1.041926626 \times 10^{12}$ . We have checked that this result was invariant under slight changes in  $s$ . From this, we see that  $\mu - \chi = 2.8 \times 10^5$  which is approximately  $0.57\sigma$ . Another information concerning the spread of the values is the difference between the largest and the smallest values of the distribution which is  $6.4\sigma$  in the present case.

There are several detailed features of this distribution which are not well understood. The first one is that the distribution is not symmetric about  $s = \frac{2}{\sqrt{c}}$ . The values of  $\chi$  spread more above  $s = \frac{2}{\sqrt{c}}$ . In addition, a more detailed study shows that the distribution is not well centered and that of values about the mean value departs more from a gaussian distribution than expected, given the number of “independent trials” (2000 in Fig. 1) made. In addition, increasing the statistics does not decrease  $\mu - \chi$  or increase significantly the difference between the largest and the smallest value. These questions are now being investigated with low  $l_{max}$  examples.

In conclusion, we have a good control on the maximal errors made as a consequence of the round-off errors. These seem not to exceed 10 times the order of magnitude given by Eq. (3.2). On the other hand, we have an incomplete understanding of their distribution within these bounds. This precludes the use of statistical methods to obtain more accurate results and other methods need to be used.

The most efficient way to improve the accuracy of  $\chi$

consists in using higher precision arithmetic. This can be done easily, for instance, using the *Mathematica* environment where one uses the instruction *SetPrecision[]* to introduce numbers with a desired number of significant digits and the instruction *Precision[]* to monitor the numerical errors. The initial precision can then be adjusted empirically in order to obtain a desired accuracy for  $\chi$ . This accuracy is then checked by making changes in  $s$  as explained above. A typical calculation with  $l_{max} = 50$ ,  $n_{max} = 200$  and a required accuracy of 16 digits in the final result takes of the order of  $10^3$  sec on a common workstation. The same type of calculation in double-precision Fortran takes about 0.1 sec. While the high-precision program runs, we could thus run the double-precision  $10^4$  times. If a proper understanding of the statistical distribution of the errors was at hand (as explained above, this is not the case), we could hope to use the  $10^4$  values to reduce  $|\delta\chi|$  by a factor  $10^{-2}$ . In the example discussed above, we would get hope to get errors in the 9-th significant digit instead of the 7-th. However, with the high-precision method we obtained 16 correct significant digits. In the example discussed above we obtain the accurate value  $\chi = 1.0419266255... \times 10^{12}$ . The difference between this more accurate value and the mean calculated above with 2000 data points is  $0.57 \times \sigma$  and stays at the same large value when the statistics is increased. In the following, the high-precision method will exclusively be used.

### C. Determination of $l_{max}$

As shown in Ref. [10], the effect of the finite truncation decays faster than exponentially with  $l_{max}$  in the symmetric phase. In general, the determination of  $l_{max}$  depends on how far we are from criticality and the required accuracy on the value calculated. In the following, we will require a 13 significant digits on  $\chi$  and  $(\beta_c - \beta)$  with  $\beta < \beta_c - 10^{-14}$ . When  $\beta = \beta_c - 10^{-14}$ , all the significant digits up to the 13-th decimal point of the quantity  $(\beta_c - \beta)$  are lost since they cancel. Consequently, in order to get 13 significant digit in  $(\beta_c - \beta)$  in the range considered, we will determine  $\beta_c$  with an accuracy of  $10^{-27}$ . This will be the most stringent requirement to determine  $l_{max}$ . As explained in the previous subsection, we can easily perform calculations with high-precision arithmetic and follow the bifurcations [10] in the ratios of successive  $a_{n,1}$  in order to determine  $\beta_c$ . Fig. 4 shows the effect of adding or subtracting  $10^{-27}$  to  $\beta_c = 1.179030170446269732511874097$  in the case of an initial Ising measure. This calculation has been performed with  $l_{max} = 50$ . If we use larger values of  $l_{max}$ ,  $\beta_c$  remains at the quoted value. This is just a particular example.

In general, the minimal value of  $l_{max}$  for which  $\beta_c$  stabilizes can be obtained from extrapolation from the changes at low  $l_{max}$  where calculations take little time.

We use the notation  $\delta\beta_c$  for  $\beta_c(l_{max}) - \beta_c$ . The quantity  $\log_{10}|\delta\beta_c/\beta_c|$  versus  $l_{max}$  is shown in Fig. 2 for the Ising model and the LG measure of Eq. (1.1) with  $m^2 = 1$ ,  $p = 2$ , and  $g = 0.1$ .

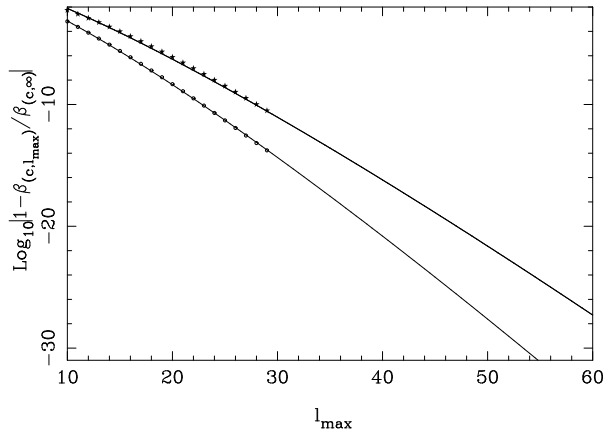


FIG. 2.  $\log_{10}|\delta\beta_c/\beta_c|$  versus  $l_{max}$  for the Ising case (circles) and the LG case (stars). The solid line is a fit with  $a + b(l_{max}\ln(l_{max}))$ .

The logarithm of the relative errors falls faster than linearly. In good approximation [10],  $\log_{10}(\Delta\beta_c) \simeq a + b(l_{max}\ln(l_{max}))$ . So if we want, say  $\delta\beta/\beta \sim 10^{-27}$ , the choices of  $l_{max} = 48$  for the Ising case and  $l_{max} = 60$  the LG cases appear to be a safe. In order to check the stability of these values, we increased the value of  $l_{max}$  to 55 in the Ising case and to 64 in the (LG) case, and we obtained the same  $\beta_c$  value in both cases. We have also checked that these values of  $l_{max}$  were sufficient to obtain 13 significant digit for  $\chi$  in the range of  $\beta$  specified above.

#### D. Effects of the Errors on the Initial Coefficients

In the Ising case,  $R_0(k) = \text{Cos}(k)$ , the initial coefficients are known analytically:  $a_{0,l} = (-1)^l/(2l)!$ . However, this is not the case in general. We want to study the effect of a change in  $\delta a_{0,l}$  in the initial coefficients on  $\beta_c$ . The results are shown in Fig. 3.

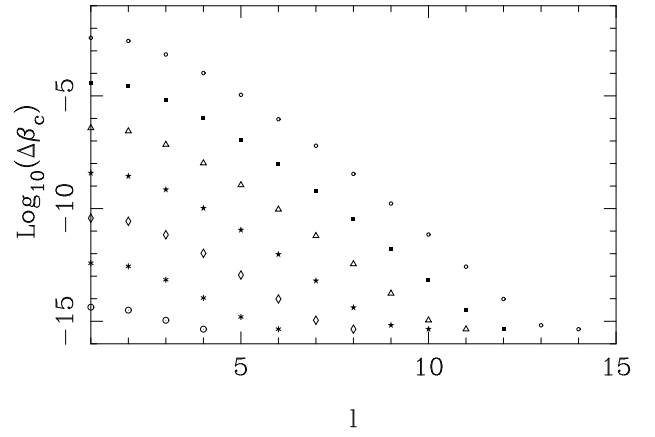


FIG. 3. The shift in  $\beta_c$ ,  $\Delta\beta_c$  as a function of the relative errors in the  $l$ -th coefficient.  $\frac{\delta a_{0,l}}{a_{0,l}} = 10^{-2}$  (empty circles),  $10^{-4}$  (filled boxes),  $10^{-6}$  (empty triangles) and so on until  $\frac{\delta a_{0,l}}{a_{0,l}} = 10^{-14}$ .

The results can be read as follows. If we are interested in determining  $\beta_c$  with, say, 10 significant digits,  $a_{0,10}$  has to be determined with 2 significant digits,  $a_{0,9}$  with 3 significant digits,  $a_{0,8}$  with 4 significant digits etc... . In the following, we are interested in universal properties (features which are independent of the measure) rather than in properties of particular measures. Consequently we have only used a double-precision calculation of the Fourier transform for the LG model. The reproducibility of the details of the calculations then require having the same  $a_{0,l}$ . On the other hand, in the Ising case, the analytical form of the initial coefficients allows a completely reproducible procedure.

#### E. What Happens in the Broken Symmetry Phase

Fig. 4 shows the existence of two phases. There are five parts of the graph we would like to discuss here.

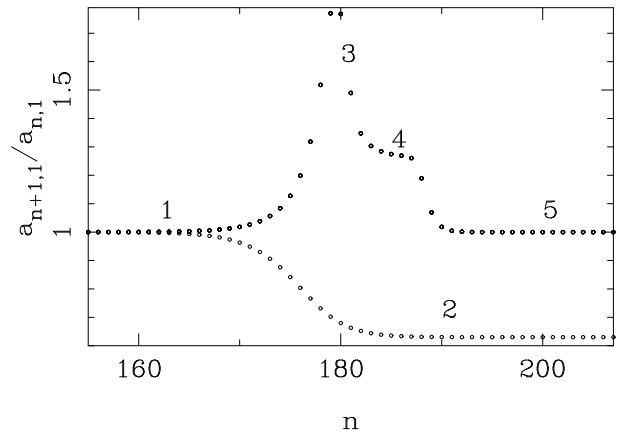


FIG. 4.  $a_{n+1,1}/a_{n,1}$  versus  $n$  for  $\beta = \beta_c \mp 10^{-27}$ .

For the rest of the discussion, it is important to specify that  $a_{n,1}$  has been calculated with the canonical value of the rescaling parameter  $s = \frac{2}{\sqrt{c}}$ . The first part is before the bifurcation. This is shown as the region “1” in Fig. 4 where the ratios of  $a_{n+1,1}/a_{n,1}$  are close to 1. The second part (“2”) shows the bifurcation in the high-temperature phase. If we are below  $\beta_c$ , the ratio  $a_{n+1,1}/a_{n,1}$  will go down to the value  $c/2$ , which guarantees the existence of a thermodynamical limit for  $\chi$  (since we need to multiply  $a_{n,1}$  by  $(\frac{2}{c})^n$  in order to get  $\chi$  see Eq.(2.10)). On the other hand, the bifurcation toward the low temperature phase is characterized by a peak shown by “3” in Fig. 4. Part 4 of the graph is a narrow “shoulder”. In the low-temperature phase, we expect  $\langle M_n^2 \rangle_n \propto 2^{2n}$ , which means  $a_{n+1,1}/a_{n,1} \simeq c \simeq 1.26$ . We studied the  $l_{max}$  dependence of this shoulder and observed that the number of points on the shoulder increases by approximately one when we increase  $l_{max}$  by 10. Unfortunately, the shoulder is not infinite and after a few iterations, the ratios will reach to 1 again (part “5”). This signals an attractive fixed point. However, this is not a fixed point of the exact (not truncated) recursion relation. This can be seen by looking at the coefficients  $a_l^*$  of these attractive fixed points for different values of  $l_{max}$ . When  $l_{max}$  increase, the values of  $a_l^*$  increase like  $(l_{max})^l$ , showing that their existence is due to the truncation process.

The fact that the truncation procedure generates numerical instabilities in the low-temperature phase can be understood from the basic formula Eq. (2.5). In the low temperature phase, the measure  $W(\phi)$  has two peaks symmetrically located with respect to the origin. At each iteration, the separation between the peaks increases by a factor 2 (in unrescaled units). By taking simple examples and going to Fourier transform, one sees that at some point the partial sums (truncated at  $l_{max}$ ) representing the exponential in Eq. (2.5) becomes inaccurate because the argument of the exponential is too large.

#### IV. CRITICAL EXPONENTS FROM FITS

In this section, we explain how to calculate the exponents  $\gamma$  and  $\Delta$  using a sequence of increasingly accurate fits of the susceptibility. The general method has been briefly outlined in Ref. [4]. Here, we give all the details of a significantly more accurate calculation which leads to a determination of  $\gamma$  with 12 decimal points. The main ingredient of the procedure is that for  $\beta$  close enough to  $\beta_c$  (i.e, for a cut-off  $\Lambda$  large enough), one can approximate very well the magnetic susceptibility (zero-momentum two point function) with an expression taking into account only the first irrelevant direction, namely :

$$\chi \simeq (\beta_c - \beta)^{-\gamma} (A_0 + A_1(\beta_c - \beta)^\Delta) . \quad (4.1)$$

The estimation of the unknown quantities in this equation proceeds in four steps. In the first step, we get a rough estimate for  $\gamma$  by using a linear fit in a range of  $\beta$  where we minimize the combined effects of the numerical errors and of the subleading corrections. In the second step, we discuss how to improve this result by estimating the sub-leading exponent  $\Delta$  and the coefficient  $A_1/A_0$ . Using these preliminary estimates, we will as the third step of the procedure, use a “bootstrap” technique between a set of high-precision data close to criticality and another set of data where the subleading corrections are important. Finally, we do a linear analysis of the difference between the fit and the high-precision data in order to get results which are as independent as possible of the slightly arbitrary choices (how to divide the data into “bins” etc... ) made during the first three steps. After this fourth step, we analyze the difference between the fit and the data away from criticality and discuss the next subleading corrections.

All the calculation of these sections have been done with either an Ising initial measure or a LG measure of the form given in Eq. (1.1) with  $m^2 = 1$ ,  $p = 2$ , and  $g = 0.1$ . We refer to these choices as the “Ising case” or the “LG case” hereafter.

##### A. Localized Linear Fits

In the first step, we calculate  $\chi$  at various temperatures and display  $\log_{10}(\chi)$  versus  $-\log_{10}(\beta_c - \beta)$ . We will use the notation

$$x \equiv -\log_{10}(\beta_c - \beta) . \quad (4.2)$$

If we display  $\log_{10}(\chi)$  versus  $x$ , we see a linear behavior with a slope  $\gamma \simeq 1.30$ . The deviations from the linear behavior are not visible to the naked eye. We need to study these deviations locally in  $\beta$ . In order to understand the corrections, we have divided the data into 14 bins of 100 points. The first bin contains the data  $x = 1.00, 1.01, \dots, 1.99$  and so on. In each bin, indexed  $i$ , we make a linear fit of  $\log_{10}(\chi)$  versus  $x$ . In the  $i$ -th bin we will call the slope  $\gamma^{(i)}$  and  $(\sigma^{(i)})^2$  denoted the sum of the squares of difference between the data and the linear fit divided by the number of points in a bin minus 2 which is ( for the  $i$ -th bin ),

$$(\sigma^{(i)})^2 = \frac{\sum_{j=1}^{100} (\log_{10}(\chi_{i,j}^{data}) - \log_{10}(\chi_{i,j}^{fit}))^2}{98} , \quad (4.3)$$

where  $j$  indexes the data points in the  $i$ -th bin. The values of  $\log_{10}(\sigma^{(i)})$  are plotted in Fig. 5.



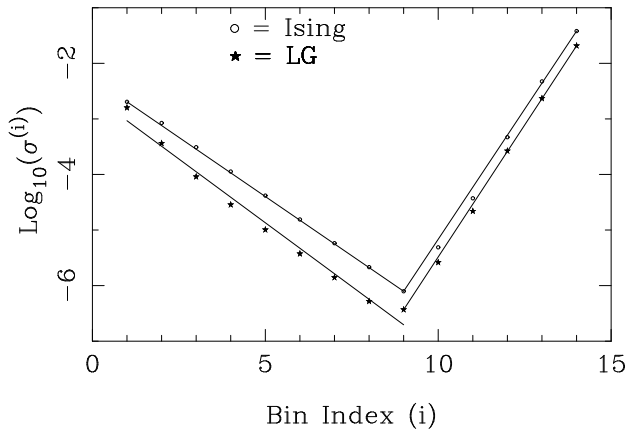


FIG. 5. The deviations from the linear fits  $\log_{10}\sigma^{(i)}$  defined in the text as function of the bin index  $i$ , for the Ising model (circles) and the Landau-Ginsburg model (stars).

It is easy to interpret this graph. There are two major sources of deviations from the linear behavior. The first one is the existence of subleading corrections to the scaling laws which decrease when  $\beta$  gets closer to  $\beta_c$ . As a first guess, we use  $\sigma^{(j)} \propto 10^{-\Delta j}$  so that  $\log_{10}\sigma^{(j)} \simeq -\Delta j + \text{constant}$ . By calculating the slopes between bin 1 and bin 9, we obtain  $\Delta \simeq 0.42$  and  $\Delta \simeq 0.45$  for the Ising and the LG cases, respectively. Thus, we already obtained a numerical value for the subleading exponent which is roughly the same for the two models considered here. The other source of deviation from the linear behavior comes from the numerical errors discussed in the previous section and which increase when  $\beta$  gets closer to  $\beta_c$  according to Eq. (3.2).  $\sigma \sim \delta/(\beta_c - \beta)$ . The slopes between bin 9 and bin 14 are  $-0.95$  and  $-0.96$  for the Ising and the LG cases, respectively, in good agreement with the  $(\beta_c - \beta)^{-1}$  dependence of the numerical errors predicted by Eq. (3.2).

In bin 9, these two deviations from linear behavior are minimized and we can consider  $\gamma^{(9)}$  as a first estimate of  $\gamma$ . Its numerical values is 1.29917 for the Ising case and 1.29914 for the LG case. By using this simple procedure we already gained almost two significant digits compared to the existing estimated [6,9] where the answer  $\gamma = 1.300$  was obtained with errors of order 1 in the last digit.

## B. Subleading Corrections

The second step consist in correcting the previous estimate by taking into account the subleading corrections. We will use the bins 6 and 7 where the next subleading corrections are reasonably small and the numerical errors are not too large. We have divided these two bins into 10 sub-bins of 100 points. We will use two digit indices for these sub-bins. For instance, sub-bin 6.5 is the fifth sub-bin of bin 6 and contains the values of  $x$ : 6.5, 6.501,

... ,6.599. Using the notation  $\bar{x}$  for the middle of the sub-bin and Eq. (4.1) we obtain,

$$\log_{10}(\chi(\bar{x})) = \gamma\bar{x} + \log_{10}(A_0 + A_1 10^{-\Delta\bar{x}}). \quad (4.4)$$

For a small change  $\delta x$  with respect to  $\bar{x}$ , we obtain that at first order in this change

$$\log_{10}(\chi(\bar{x} + \delta x)) - \log_{10}(\chi(\bar{x})) = (\gamma - \frac{A_1}{A_0} \Delta 10^{-\Delta\bar{x}}) \delta x + \vartheta(\delta x^2). \quad (4.5)$$

The coefficient of  $\delta x$  can be interpreted as the local slope near  $\bar{x}$ . Indexing each sub-bin by  $j$  (e.g  $j : 6, 6.1, 6.2...$ ) and its middle by  $j + 0.0495$  (e.g. 6.1495 is the middle of the sub-bin 6.1), the the slope  $\gamma^{(j)}$  in the sub-bin  $j$  reads

$$\gamma^{(j)} \simeq \gamma - \Delta \left( \frac{A_1}{A_0} \right) 10^{-\Delta(j+0.0495)}. \quad (4.6)$$

The unknown quantities  $\frac{A_1}{A_0}$  and  $\Delta$  can be obtained from linear fits of  $\log_{10}(|\gamma^{(j+0.1)} - \gamma^{(j)}|)$  versus  $j$ . From Fig. 6, one can see that in good approximation, there exists an approximate relationship between these two quantities in the two cases considered. In addition, the slope appears to be identical for the two cases.

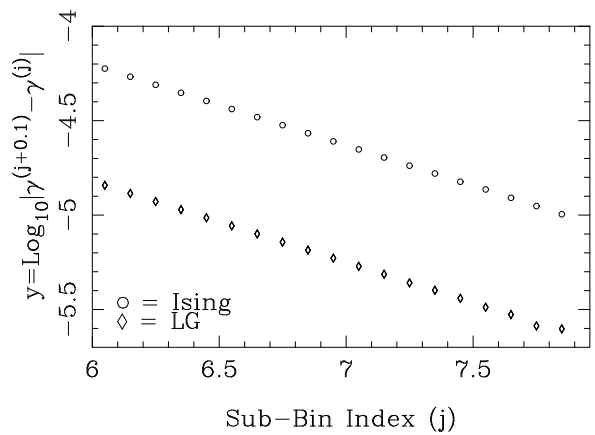


FIG. 6. The linear fits of  $\log_{10}(|\gamma^{(j+0.1)} - \gamma^{(j)}|)$ , for the Ising case (circles) and for the LG case (stars).

The slope and the intercept can be calculated from Eq. (4.6) which implies that

$$\log_{10}(|\gamma^{(j+0.1)} - \gamma^{(j)}|) \simeq -\Delta(j + 0.0495) + \log_{10}(\Delta \left| \frac{A_1}{A_0} \right|) + \log_{10}(1 - 10^{-0.1\Delta}). \quad (4.7)$$

The subleading exponent  $\Delta$  is the absolute value of the slope. Having determined  $\Delta$  and knowing the intercept we can then determine  $\log_{10}(\left| \frac{A_1}{A_0} \right|)$ . Using this procedure, we obtained  $A_1/A_0 = -0.57$  and  $\Delta = 0.428$  for the Ising case and  $A_1/A_0 = 0.14$  and  $\Delta = 0.427$  for the LG case.

If we now repeat the first step - a linear fit in bin 9 - but with  $\chi$  divided by  $[1 + (A_1/A_0)(\beta_c - \beta)^\Delta]$ , we obtain  $\gamma = 1.299141 \mp 10^{-6}$  for the two models considered above. Given that for a calculation using double precision in bin 9 we have values of  $\chi$  with between 6 and 7 significant digits, this estimate seems to be the best result we can obtain with this procedure (see the discussion of the numerical errors in section III.B).

### C. A Bootstrap Procedure Involving Higher Precision Data

Up to now, our desire to minimize the subleading corrections which decay like  $10^{-\Delta x}$  has been contradicted by the appearance of numerical errors growing like  $10^{-(16+x)}$ . However, we have explained in section III.B, that it is possible to circumvent this difficulty by using an arithmetic having a better precision than the usual double precision. In this subsection, we will use data having at least 13 correct significant digits in bin 11, 12 and 13. We call this data “high precision data”. As we explained before, we choose  $l_{max} = 50$  and  $l_{max} = 58$  for the Ising and the LG case, respectively.

Since the calculations are more lengthy, we used only 10 points in each bin. We also determined  $\beta_c$  with 27 significant digit so that in bin 13, the subtracted quantity  $(\beta_c - \beta)$  is also known at least with 13 significant digit. We found  $\beta_c = 1.179030170446269732511874097$  for the Ising case and  $\beta_c = 1.14352915687979895500964720$  for the LG case. We then use bin 13 (where the subleading corrections are small and the errors are not very important) to calculate  $\chi$  divided by the subleading correction as explained in the previous subsection to estimate  $\gamma$ . Then with the new value of  $\gamma$  obtained we go back to bin 7 to calculate the subleading corrections. This procedure can be iterated and this ‘bootstrap’ of linear fits converges rapidly. We obtain  $\gamma = 1.299140732$ ,  $\Delta = 0.4262$  and  $A_1/A_0 = -0.564$  for the Ising model and  $\gamma = 1.299140730$ ,  $\Delta = 0.4258$  and  $A_1/A_0 = 0.135$  for the LG case. These numbers change typically by one in the last digit quoted above if one replaces bin 7 by bin 6 to evaluate  $\Delta$ . In order to remove this arbitrariness, we will now use these numbers as the initial values for a more accurate procedure.

### D. Linear Analysis of the Discrepancies

We have now reduced the errors made in the estimate of the unknown quantities appearing in Eq. (4.1) to a sufficiently low level to allow us to treat these errors in a linear approximation. We start with an initial fit of the data, for instance as obtained in step 3, with errors in the unknown quantities parametrized in the following way:

$$[\log_{10}\chi]_{fit} = \log_{10}A_0 + \delta(\log_{10}A_0) + (\gamma + \delta\gamma)x + \log_{10}(1 + (c_1 + \delta c_1)10^{-(\Delta + \delta\Delta)x}) . \quad (4.8)$$

where  $c_1 \equiv A_1/A_0$  and  $\gamma, \Delta$  stand for the exact values. On the other hand, we assume that the data can be fitted according to Eq. (4.1)

$$[\log_{10}\chi]_{data} = (\log_{10}A_0 + \gamma x + \log_{10}(1 + c_1 10^{-\Delta x})) . \quad (4.9)$$

Combining the two above equations we obtain at first order

$$[\log_{10}\chi]_{fit} - [\log_{10}\chi]_{data} \simeq \delta(\log_{10}A_0) + \delta\gamma x + \frac{\delta c_1 10^{-\Delta x}}{\ln(10)} - c_1 10^{-\Delta x} x \delta\Delta . \quad (4.10)$$

Interestingly, the  $x$ -dependences of the four terms are all distinct and we can fit  $\delta(\log_{10}A_0)$ ,  $\delta\gamma$ ,  $\delta c_1$  and  $\delta\Delta$  using a standard least square procedure where the function to be fitted depends *linearly* on the fitted parameters. This procedure can be repeated until some numerical stability is achieved. The final results are insensitive to small changes in the initial values coming from the uncertainties associated with the previous step. Using bin 13, we obtain  $\gamma = 1.2991407301599$  and  $\Delta = 0.4259492$  for the Ising model, and,  $\gamma = 1.2991407301582$  and  $\Delta = 0.4259478$  for the LG case. The small numerical fluctuations which persist after many iterations produce changes of less than 2 in the last quoted digit. The origin of these small fluctuations can be inferred by plotting  $[\log_{10}\chi]_{fit} - [\log_{10}\chi]_{data}$  for the final fit (see Figs. 7 and 8 in the next section). The non-smoothness of these differences in bin 13 indicates that they are due to the numerical errors on  $\chi$ . The amplitude of these differences is smaller than  $10^{-13}$  consistently with the fact that we performed the calculation of  $\chi$  in a way that guaranteed at least 13 accurate significant digits. These fluctuations are indicative of the limitation in the numerical precision of our procedure. The accuracy of the value of the exponents, i.e. how close they are to the “true” values, is further limited by the fact that there exist corrections to our main assumption Eq. (4.1). If we assume universality, the discrepancy between the values of the exponents for the two cases considered should give us an indication concerning the accuracy of the results. For instance, the discrepancy between the two estimates of  $\gamma$  is of order  $10^{-12}$  which is about ten times larger than the fluctuations of numerical origin. The estimation of the next sub-leading corrections is the main topic of the next section.

## V. THE NEXT SUB-LEADING CORRECTIONS

In the previous section, we have used the parametrization of Eq. (4.1) for the susceptibility near criticality.

This parametrization is by no means exact and corrections become more sizable as we move away from criticality. The corrections come from effects which can be calculated by a linearization procedure (the next irrelevant directions, see subsection IID) or effects which are intrinsically non-linear. Anticipating the results which will be presented in the next section, we obtain the approximate values  $\Delta_2 \simeq 0.43$  (we recall that since we only took into account one irrelevant direction, we used the notation  $\Delta$  for  $\Delta_2$  before) and  $\Delta_3 \simeq 2.1$ . In other words if we consider the first irrelevant direction as “first order”, the next irrelevant directions produce effects which are smaller than the fourth order. In bin 13, these effects are completely unnoticeable in our analysis. The nonlinear effects are discussed in the subsection V A. The main result obtained there is that all the corrections can be parametrized in the following way:

$$\chi \simeq (\beta_c - \beta)^{-\gamma} (A_0 + A_1(\beta_c - \beta)^\Delta + A_2(\beta_c - \beta)^{2\Delta} + A_a(\beta_c - \beta) + \dots), \quad (5.1)$$

In the next subsection, we analyze the data in terms of the new parametrization and extrapolate our results in order to estimate the errors made in the calculations of  $\gamma$  and  $\Delta$  in the previous section.

### A. Nonlinear Corrections

The previous analysis, describes the linearized flows near the fixed point. The closer to criticality we are, the more iterations are spent close to the fixed point and the more accurate the linear description is. Nevertheless, when we approach or leave the fixed point, nonlinear effects are unavoidable. These nonlinear effects can be studied more easily in low-dimensional maps. Without entering into the detail of this analysis [11], we can envision three types of corrections which we now proceed to discuss.

As already noticed in [9], the “constants”  $A_0$  and  $A_1$ , should be replaced by functions  $A_i((\beta_c - \beta))$  such that  $A_i(\lambda_1(\beta_c - \beta)) = A_i(\beta_c - \beta)$ . This invariance implies an expansion in integral powers of  $(\beta_c - \beta)^{i\omega}$  (Fourier modes) with  $\omega = \frac{2\pi}{\ln(\lambda_1)} \simeq 17.8$ . We argue here that the coefficients of the non-zero powers are suppressed by 14 orders of magnitude. The rationale for this suppression is that the non-zero modes contribute to the extrapolated slope (an asymptotic estimator for  $\gamma - 1$  used with the high-temperature expansion) with about the same strength as the zero mode [9]. However, this is the result of a double amplification for the non-zero modes. This results from the equations (3.7) to (3.10) of Ref. [9]. First, when calculating the coefficients of high temperature expansion one gets an amplification factor of order  $|\Gamma(\gamma + i\omega)| \simeq 5 \times 10^{10}$ . Second, while calculating the extrapolated slope, one gets another amplification by a factor  $\omega^3 \simeq 5 \times 10^3$ . Putting these two factor together,

we obtain the claimed 14 orders of magnitude. Such a small effect is smaller than our numerical resolution.

Second, the singularity  $(\beta_c - \beta)^{-\gamma}$  should be replaced by  $((\beta_c - \beta) + d_2(\beta_c - \beta)^2 + \dots)^{-\gamma}$  with coefficients  $d_l$  calculable in low dimensional maps. These corrections generate *analytical* corrections to the scaling law in contrast to the subleading corrections which are in general not integer powers

Third the nonlinear corrections associated with the irrelevant directions generate corrections which are presumably of the form  $(\beta_c - \beta)^{l\Delta}$  with  $l = 2, 3, \dots$ . Later we call these corrections the quadratic corrections or the second order effects.

In summary, the corrections associated with nonlinear contributions obey the parametrization of Eq. (5.1) for a sequence of exponents 0.43, 0.86, 1, 1.29, 1.72, 2,  $\dots$ . Note that these exponents are very close to each other and it may be difficult to disentangle their effects.

### B. Empirical Determination of the Corrections

We are now ready to use the data to determine some of the unknown quantities in Eq. (5.1). In the following, we will study these corrections for the Ising and the LG cases separately. The reason for doing this is that in the Ising case, the ratio  $A_1/A_0 = -0.56$  while in the LG case,  $A_1/A_0 = 0.14$ . The relative size of the quadratic corrections is presumably of order  $(A_1/A_0)^2$  and these corrections will be more sizable in the Ising case. We start with the assumption that there is one next sub-leading correction which dominates when we move from bin 13 to smaller values of  $x$ . In other words,

$$\chi 10^{-\gamma x} - A_0 - A_1 10^{(-\Delta x)} \simeq A 10^{-\phi}, \quad (5.2)$$

in an intermediate  $x$  region. In this equation, the four parameters  $\gamma$ ,  $\Delta$ ,  $A_0$  and  $A_1$  are understood as their best estimates near criticality obtained in the previous section. Anticipating the results obtained below, the exponent  $\phi$  is roughly of order one. The corrections in bin 8 are thus of order  $10^{-8}$  which is precisely of the same order as the numerical errors if we use double-precision calculations. Consequently we had to use the *Mathematica*-based method described in the section III B in order to get at least 4 significant digits for the corrections. For time considerations, we have limited our calculations to 10 points per bin.

If Eq. (5.2) is approximately correct, the logarithm of the l.h.s. should be approximately linear in some region of  $x$ . This quantity is displayed in Fig. 7 for the Ising model and in Fig. 7 for the LG model.

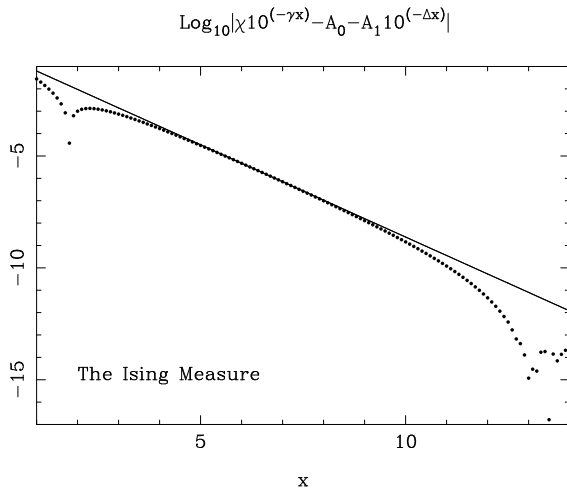


FIG. 7.  $\log_{10}[|\chi 10^{(-\gamma x)} - A_0 - A_1 10^{(-\Delta x)}|]$  versus  $x = -\log_{10}(\beta_c - \beta)$  for the Ising measure.

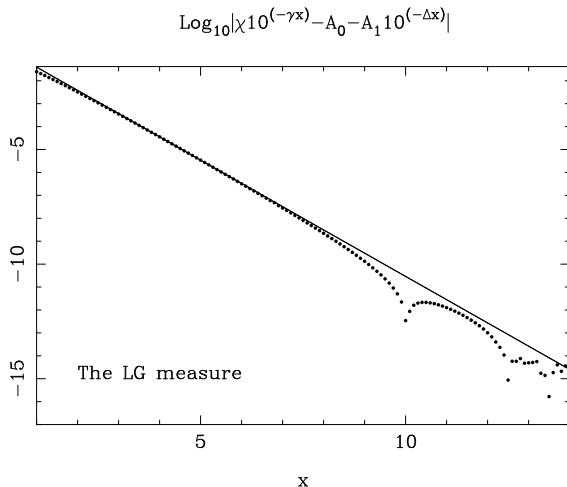


FIG. 8.  $\log_{10}[|\chi 10^{(-\gamma x)} - A_0 - A_1 10^{(-\Delta x)}|]$  versus  $x = -\log_{10}(\beta_c - \beta)$  for the LG measure.

One sees that in both case the graph is approximately linear over a large region of  $x$ . Using a linear fit in each of the bins of these regions we obtain  $\phi = 0.82$  and  $A = 0.4$  with  $\sigma = 9 \times 10^{-4}$  in bin 6 for the Ising model and  $\phi = 1.01$  and  $A = 0.4$  with  $\sigma = 6 \times 10^{-4}$  in bin 4 for the LG model. Other bins have larger values of  $\sigma$  and values of  $\phi$  which change by a few percent while moving from bin to bin.

In the Ising case, we have  $|\frac{A}{A_0}| \approx (\frac{A_1}{A_0})^2$  and  $\phi \simeq 2\Delta$  and we interpret this as a second order (or quadratic) effect associated with the first irrelevant corrections. In other words,  $A \simeq A_2$  if we follow the notations of Eq.(5.1). In the LG case  $(\frac{A_1}{A_0})^2 \simeq 0.02$  is very small and the dominant effect in the linear region is the analytic correction ( $\phi = 1$ ) behavior. In other words,  $A \simeq A_a$  used if we

follow again the notations of Eq. (5.1).

The departure from linearity occurs in its most extreme way as dips located near  $x = 2$  in the Ising case and  $x = 10$  in the LG case. These dips signal the existence of effects of opposite signs. A plausible interpretation of the location of these dips is that they occur at values of  $x$  where the  $10^{-2\Delta x}$  prevail over the  $10^{-x}$  analytical corrections. A detailed analysis confirms this view for the Ising model, which allows us to neglect the analytical corrections in bin 13. For the LG model, two effects compete in bin 10 which is dangerously close to bin 13 where the parameters are fined-tuned (see below) and we were unable to get a clear linear behavior after one more subtraction. Our most plausible explanation is the following for the LG model. Near  $x = 10$ , we have  $A_a 10^{-x} \simeq -A_2 10^{-2\Delta x}$  which implies  $A_2 \simeq 0.016$ . With this rough estimates  $|\frac{A_2}{A_0}| \approx (\frac{A_1}{A_0})^2$  which is consistent with a second order effect. So if this interpretation is correct the quadratic effects are about twice the size of the analytic corrections in bin 13 for the LG model.

In summary, we will use the assumption that in bin 13, the corrections are mostly second order effects and we will neglect the analytical corrections. This assumption is well-obeyed in the Ising case but is just an order magnitude estimate in the LG case.

### C. Accuracy of the Previous Estimate

We are now in position to estimate the effects of the next subleading corrections in the calculation of the critical exponents reported in the previous section. First of all, we notice that by extrapolating the dominant linear behavior described in the previous subsection to bin 13, we obtain effects smaller than  $10^{-11}$  in the Ising case and smaller than  $10^{-13}$  in the LG case. This justifies treating them as small perturbations in bin 13. When we fitted the data in bin 13 without taking these small effects into account, we made small adjustments in the fitted parameters which allowed us to fit the data with a precision comparable to the numerical precision. In order to get a rough estimate of how much the next subleading corrections led us to misestimate the exponents, we can linearize the next subleading corrections about  $x = 13$ . We obtain a change of the “apparent” slope:

$$|\delta\gamma| \approx \left| \frac{A}{A_0} 10^{-13\phi} \phi \right|. \quad (5.3)$$

The order of magnitude of the corresponding errors on  $\Delta$  can be estimated by equating the term linear in  $\delta\gamma$  with the term linear in  $\delta\Delta$  in Eq. (4.10). This yields:

$$|\delta\Delta| \approx \left| \frac{A_0}{A_1} 10^{-13\Delta} \delta\gamma \right|. \quad (5.4)$$

We insist that this is only an order of magnitude estimate. Plugging numerical values, we obtain  $|\delta\gamma| = 3 \times 10^{-12}$  and  $|\delta\Delta| = 2 \times 10^{-6}$  in the Ising case, and,

$|\delta\gamma| = 2 \times 10^{-13}$  and  $|\delta\Delta| = 6 \times 10^{-7}$  in the LG case. In the Ising case, the estimated errors are slightly larger than the discrepancies between the values obtained with the two measures. In the LG case, the estimated errors are slightly smaller. However, larger uncertainties in the error estimates appeared in the LG case. If we use the largest estimates for the errors, our final result for the first method is:

$$\gamma = 1.299140730159 \pm 3 \times 10^{-12} \quad (5.5)$$

$$\Delta = 0.4259485 \pm 2 \times 10^{-6} . \quad (5.6)$$

## VI. THE EIGENVALUES OF THE LINEARIZED RG TRANSFORMATION

As explained above, the easiest way to calculate the critical exponents consists in linearizing the RG transformation near a fixed point  $R^*(k)$  specified by the coefficients  $a^*_l$ . This can be done as follows. First we express the coefficients after  $n$  iterations in terms of small variations about the fixed point:

$$a_{n,l} = a_l^* + \delta a_{n,l} . \quad (6.1)$$

At the next iteration, we obtain the linear variations

$$\delta a_{n+1,l} = \sum_{m=1}^{l_{max}} M_{l,m} \delta a_{n,m} . \quad (6.2)$$

The  $l_{max} \times l_{max}$  matrix appearing in this equation is

$$M_{l,m} = \frac{\partial a_{n+1,l}}{\partial a_{n,m}} , \quad (6.3)$$

evaluated at the fixed point.

Approximate fixed points can be found by approaching  $\beta_c$  from below and iterating until the ratio  $a_{n+1,1}/a_{n,1}$  takes a value which is as close as possible to 1. This procedure is described in Ref. [4]. The approximated fixed points obtained with this procedure depend on  $\beta_c$ . Using their explicit form which we denote  $R^*(k, \beta_c)$ , we obtained a universal function  $U(k)$  by absorbing  $\beta$  into  $k$ . More explicitly, we found that

$$U(k) = R^*(\sqrt{\beta_c}k, \beta_c) , \quad (6.4)$$

is in very good approximation independent of the model considered. This function is related to a fixed point  $f(s^2)$  constructed in Ref. [7] by the relation

$$U(k) \propto f\left(\left(\frac{c-4}{2c}\right)k^2\right) . \quad (6.5)$$

The Taylor coefficients of  $f$  can be found in the file `approx.t` in [7]. Normalizing Eq.(6.5) with  $U(0) = 1$ , we obtain

$$U(k) = 1. - 0.35871134988k^2 + 0.0535372882k^4 - \dots . \quad (6.6)$$

It is not known if there is only one non-trivial fixed point for Dyson's model. Using the parametrization of Eq. (1.1), we have considered [4] the 12 cases obtained by choosing among the following possibilities:  $m^2 = \pm 1$  (single or double-well potentials),  $p = 2, 3$  or  $4$  (coupling constants of positive, zero and negative dimensions when the cut-off is restored) and  $g = 10$  or  $0.1$  (moderately large and small couplings). All approximate fixed points we have constructed give a function  $U(k)$  very close to Eq. (6.6). The closeness can be characterized by the  $\rho$ -norms introduced in [7]. For  $\rho = 2$  and  $l \leq 42$  we found that the error  $\delta u_l$  on the  $l$ -th coefficients of the approximate  $U(k)$  with respect to the accurate expression obtained from Ref. [7] were bounded by  $|\delta u_l| < \frac{5 \times 10^{-5}}{l!2^l}$  for calculations using double precision. In other words, the function  $U(k)$  seems to be independent of the general shape of the potential, the strength of the interactions and whether or not the model is perturbatively renormalizable.

Using these approximate fixed points, we were able to obtain  $\gamma$  and  $\Delta$  with 7 decimal points. In the following, we will use directly the more precise function  $U(k)$  constructed by Koch and Wittwer [7]. We retained 16 significant digits for the coefficients appearing in Eq. (6.6) and used values of  $l_{max}$  up to 65. We then calculated the eigenvalues of the matrix given in Eq. (6.3) with two different methods. The first was using "blindly" the instruction *Eigenvalues* in *Mathematica*. The second consisted in using the eigenvalue routine *LAPACK* [12] for which we were able to vary the control parameters of the program. The two methods gave identical results with 14 decimal points for the first two eigenvalues. The first six eigenvalues are given below.

$n$	$\lambda_n$
1	1.42717247817759
2	0.859411649182006
3	0.479637305387532
4	0.255127961414034
5	0.131035246260843
6	0.0654884931298533

In order to get an idea regarding the asymptotic behavior of the eigenvalues, a larger set of values is displayed in Fig. 9.

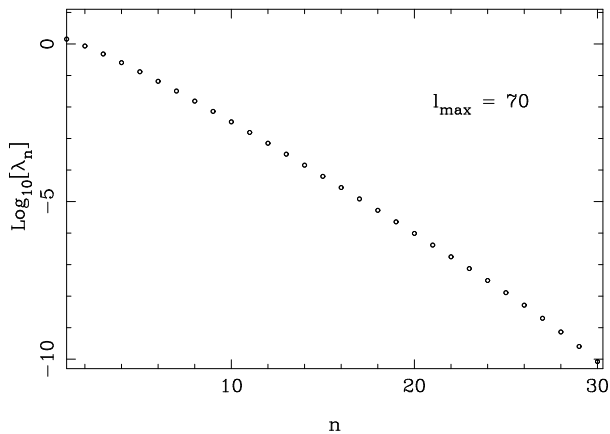


FIG. 9.  $\log_{10}[\lambda_n]$  versus  $n$ .

It is clear from the figure that  $\lambda_n$  falls faster than exponentially with  $n$ . This property is important when the non-linear effects are calculated.

Using the first two eigenvalues and the relationship between the eigenvalues and the exponents reviewed in the previous section, we obtain the values

$$\gamma = 1.2991407301586 \pm 10^{-13} \quad (6.7)$$

$$\Delta = 0.4259468589881 \pm 10^{-13} . \quad (6.8)$$

The (conservative) estimation of the errors is based on errors of order  $10^{-14}$  on the eigenvalues and the fact that the derivatives of the exponents with respect to the eigenvalues yields factors less than 4.

## VII. CONCLUSIONS AND PERSPECTIVES

In conclusion, we have calculated the exponents  $\gamma$  and  $\Delta$  with a accuracy significantly better than in Ref. [4]. The three independent calculations performed here agree on the following value for the leading exponent:

$$\gamma = 1.299140730159 \pm 10^{-12} . \quad (7.1)$$

Our results show the excellent agreement between the methods developed in Ref. [10] and an expansion about the fixed point of Ref. [7]. As far as the calculation of the exponents are concerned, the linearization procedure is much simpler and more accurate.

It is important to know if the non-universal quantities  $A_0, A_1, A_2, A_a, \dots$  could also be calculated by a using an expansion about the fixed point which involves non-linear terms. We have addressed this question in a simplified model, namely the recursion relation for the susceptibility

$$\chi_{n+1} = \chi_n + \beta \left(\frac{c}{2}\right)^{n+1} \chi_n^2 \quad (7.2)$$

A detailed analysis [11], shows that in this model, the unknown quantities appearing in the scaling law for  $\chi$  are

completely calculable. If the procedure can be extended to the hierarchical model, then we could almost consider the model as solvable.

Assuming that the non-universal quantities can be calculated in a reasonably simple way for all the renormalized quantities, we would be in position to decide if the introduction of the bare parameters can be replaced by a choice of non-universal quantities appearing in the scaling laws. If we knew the range of these non-universal quantities and their mutual dependence, we could just input an “independent set” and obtain directly all the scaling laws. In particular, in  $D = 4$ , this procedure would yield triviality bounds. This alternate way of using input parameters in field theory is now being investigated.

## ACKNOWLEDGMENTS

This research was supported in part by the Department of Energy under Contract No. FG02-91ER40664. J.J. Godina is supported by a fellowship from CONACYT. Y.M. thanks P. Wittwer and the CERN lattice group for useful conversations, the CERN theory division for its hospitality while this work was initiated, and the Aspen Center for Physics, where this manuscript was in part written, for its stimulating environment. M.B.O. thanks the CERN theory division for its hospitality while this work was initiated.

- 
- [1] K. Wilson, Phys. Rev. B. **4**, 3185 (1971) ; Phys. Rev. D **3**, 1818 (1971); K. Wilson and J. Kogut, Phys. Rep. **12**, 75 (1974); K. Wilson, Phys. Rev. D **6**, 419 (1972).
  - [2] F. Dyson, Comm. Math. Phys. **12**, 91 (1969) ; G. Baker, Phys. Rev. B**5**, 2622 (1972).
  - [3] G. Parisi, *Statistical Field Theory*, (Addison Wesley, New York, 1988).
  - [4] J.J. Godina, Y. Meurice, M.B. Oktay Phys. Rev. D **57**, R6581 (1998).
  - [5] Y. Meurice and G. Ordaz, J. Phys. A **29**, L635 (1996).
  - [6] P. Bleher and Y. Sinai, Comm. Math. Phys. **45**, 247 (1975) ; P. Collet and J. P. Eckmann, Comm. Math. Phys. **55**, 67 (1977); G. Baker and G. Golner, Phys. Rev. B **16**, 2801 (1977); D. Kim and C. Thomson, J. Phys. A **10**, 1579 (1977); H. Koch and P. Wittwer, Comm. Math. Phys. **106**, 495 (1986) , **138**, (1991) 537 , **164**, (1994) 627.
  - [7] H. Koch and P. Wittwer, Math. Phys. Electr. Jour. (<http://www.ma.utexas.edu/mpej/MPEJ.html>), **1**, Paper 6 (1995).
  - [8] Y. Meurice and G. Ordaz, J. Stat. Phys. **82**, 343 (1996).
  - [9] Y. Meurice, G. Ordaz and V. G. J. Rodgers, Phys. Rev. Lett. **75**, 4555 (1995); Y. Meurice, S. Niermann, and G. Ordaz, J. Stat. Phys. **87**, 363 (1997).

- [10] J.J. Godina, Y. Meurice, M.B. Oktay and S. Niermann, Phys. Rev. D **57**, 6326 (1998).
- [11] Y. Meurice and S. Niermann, Univ. of Iowa preprint 25-9804, in preparation.
- [12] E. Anderson et al., *Lapack User's Guide*, <http://www.netlib.org/lapack/lug> .